**Rare Metal Materials and Engineering**
Volume 52, Issue 6, June 2023
Available online at www.rmme.ac.cn

Science Press

**Cite this article as**: Jing Zhenquan, Sun Yanhui, Chen Lian, et al. Numerical Simulation of Current, Magnetic Field and Electromagnetic Force in Vacuum Arc Remelting of Titanium Alloy[J]. Rare Metal Materials and Engineering, 2023, 52(06): 1994-2001.

ARTICLE

# Numerical Simulation of Current, Magnetic Field and Electromagnetic Force in Vacuum Arc Remelting of Titanium Alloy

**Jing Zhenquan[1], Sun Yanhui[1], Chen Lian[2], Geng Naitao[3], Zheng Youping[3], Peng Li[3], Wang Ying[3]**

*[1] Collaborative Innovation Center of Steel Technology, University of Science and Technology Beijing, Beijing 100083, China; [2] Pangang Group Panzhihua Research Institute of Iron and Steel Co., Ltd, Panzhihua 617000, China; [3] Chengdu Advanced Metal Materials Industrial Technology Research Institute Co., Ltd, Chengdu 610300, China*

**Abstract:** The Maxwell 3D module in Ansys Electromagnetics Suite was used to establish a mathematical and physical model for electromagnetic field in the vacuum arc remelting process of titanium alloy, and the interaction law of current, magnetic field and electromagnetic force in the melting process was analyzed. The results show that the current in the ingot is centripetal and concentrated within 350 mm of the upper part of the ingot. Tangential magnetic field is generated by smelting current and axial magnetic field is generated by stirring current, which are simply coupled. Under the action of smelting current and its self-induced magnetic field, radial and axial electromagnetic forces are generated; the electromagnetic force rotates under the action of the stirring magnetic field, generating tangential electromagnetic force. With the change of smelting current, the tangential component of magnetic field and the radial and axial resultant force of electromagnetic force change linearly. The axial component of the magnetic field and the radial component of the electromagnetic force change linearly with the stirring current.

**Key words:** titanium alloy; vacuum arc remelting; numerical simulation; electromagnetic field; electromagnetic force

Because titanium alloy has a series of remarkable advantages such as high specific strength, good corrosion resistance and high melting point, it has been widely used in aerospace, equipment manufacturing, medical equipment, sporting goods and other fields[1]. Vacuum arc remelting (VAR) is currently the main production method for titanium alloy ingots. It has the advantages of low equipment investment and operation cost, simple operation, etc[2–3].

VAR is a metallurgical production process in which an arc is formed by low voltage and high current is used as a heat source to smelt metals and to produce ingots under vacuum conditions[2–4]. The arc is composed of hot electrons emitted from cathode and plasma formed after ionization of gas. The stability of the arc is very important for VAR. When the gas pressure and other process parameters in the furnace are not well controlled, the arc will deflect and burn through the crucible seriously, resulting in serious accidents. In order to converge the arc, the external magnetic field is often used to stabilize the arc[5–6]. The current in the molten pool is affected by the magnetic force of the external magnetic field, which makes the current carrying metal in the molten pool rotate and produce stirring effect. Proper stirring can make the temperature and composition of the molten pool uniform, refine the ingot grain, reduce the internal defects of the ingot and improve the surface quality of the ingot. However, if the stirring is too strong, it will deteriorate the quality of the ingot. The electromagnetic force generated by the interaction between the melting current and its self-induced magnetic field also has an important influence on the molten pool flow, the structure and composition uniformity of the ingot[7].

It is difficult to observe and to detect the physical and chemical phenomena and ingot morphology of VAR process, and the cost of production test is very high, so the numerical simulation becomes the main method. In this study, the

Received date: October 20, 2022
Corresponding author: Sun Yanhui, Ph. D., Professor, Collaborative Innovation Center of Steel Technology, University of Science and Technology Beijing, Beijing 100083, P. R. China, E-mail: ustbsyh801@163.com

Maxwell 3D module of Ansys Electromagnetics Suite was used to establish the mathematical and physical model for electromagnetic field in VAR process of titanium alloy, and the interaction law of current, magnetic field and electromagnetic force in the smelting process was analyzed and mastered, so as to provide a theoretical guidance for the production process of VAR[8–10].

## 1 Mathematical Model

In the process of VAR of titanium alloy, the induced magnetic field is mainly generated by melting current and stirring current. The induced magnetic field and melting current interact to produce electromagnetic force, that is, Lorentz force, which promotes the flow of liquid metal. The control of electromagnetic field and electromagnetic force is mainly described by Maxwell's equations.

### 1.1 Governing equations

The main equations used in the model are as follows[11]:

Gauss's law

$$\nabla \times B = 0 \tag{1}$$

Ampere's law:

$$J = \nabla \times \frac{B}{\mu} \tag{2}$$

Faraday's law:

$$\nabla \times E = -\frac{\partial B}{\partial t} \tag{3}$$

Ohm's law:

$$J = \sigma E \tag{4}$$

where $\nabla = \frac{\partial}{\partial x}\vec{i} + \frac{\partial}{\partial y}\vec{j} + \frac{\partial}{\partial z}\vec{k}$; $B$ is the magnetic flux density, T; $J$ is the induced current density, $A \cdot m^{-2}$; $E$ is the electric field strength, $V \cdot m^{-1}$; $t$ is time, s; $\mu$ is the magnetic permeability, $H \cdot m^{-1}$; $\sigma$ is the electrical conductivity, $S \cdot m^{-1}$.

### 1.2 Assumptions and simplified mathematic model

To simplify the model reasonably, the following assumptions are made[12].

1) The stirring coil is simplified as a conductive region of the same volume.

2) The surface of molten pool is assumed to be plane, and the influence of liquid metal flow on magnetic field is ignored.

3) Since the relative permeability of crucible cooling water and stainless steel protective sleeve is close to 1, they are treated as air domain in the model.

4) The crucible, ingot and electrode are regarded as isotropic materials, and their physical parameters such as bulk conductivity and relative permeability are set as constants.

5) The arc area is regarded as a conductor with a certain resistance, and its resistivity is calculated by Ohm's law.

### 1.3 Boundary conditions and calculating parameters

1) The magnetic flux parallel boundary condition was applied to the external surfaces of the surrounding air zone.

2) The stirring coil was loaded with current density ($j$) according to the following equation:

$$j = \frac{NI}{A} \tag{5}$$

where $N$ is the number of coil turns; $I$ is stirring current, A; $A$ is the cross-sectional area of the coil, $m^2$.

3) The melting current was loaded with the top of the crucible as the positive electrode and the top of the electrode as the negative electrode.

The mathematical model of VAR electromagnetic field mainly includes crucible, stirring coil, ingot, electrode, arc and air domain[13–14]. Its structure is shown in Fig.1.

The Maxwell 3D module of Ansys Electromagnetics Suite was used to perform the calculations. Tetrahedral meshes were used in the computational domain, mesh adaptive techniques were used for mesh encryption, and finer meshes were used for crucible, electrode, and ingot to improve computational accuracy. Detailed parameters of the model are shown in Table 1, and physical parameters used in model calculation are shown in Table 2.

## 2 Model Validation

In order to compare the calculation results of stirring magnetic field with the actual measurement results, a Gauss meter was used to measure the magnetic field intensity without ingot in the crucible every 200 mm along the central axis. Fig. 2 shows the comparison between the calculated and measured magnetic field strength in the central axis of the crucible when

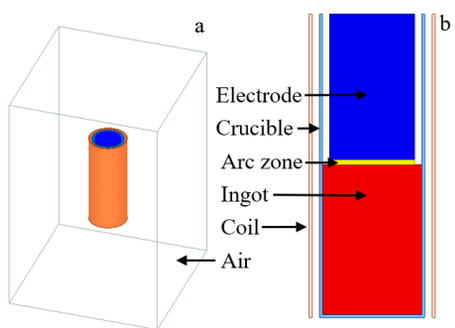


Fig.1 Schematic diagram of VAR electromagnetic field model: (a) whole model and (b) longitudinal section of the model (excluding air domain)

**Table 1 Calculation parameters of electromagnetic field model**

| Parameter | Value |
|---|---|
| Ingot diameter/mm | 660 |
| Ingot height/mm | 1000 |
| Electrode diameter/mm | 570 |
| Electrode height/mm | 970 |
| Crucible diameter/mm | 700 |
| Crucible height/mm | 2000 |
| Stirring coil diameter/mm | 800 |
| Arc zone height/mm | 30 |
| Melting current, $I_m$/kA | 21, 22, 23 |
| Stirring current, $I_s$/A | 8, 9, 10 |

**Table 2 Electromagnetic property parameters of materials[9 - 10]**

| Material | Value | |
|---|---|---|
| | Bulk conductivity/S·m$^{-1}$ | Relative permeability |
| Ingot, electrode | 1.82×10$^6$ | 1.000 18 |
| Coil, crucible | 5.8×10$^7$ | 0.999 991 |
| Arc zone | 656.72 | 1 |
| Air domain | 0 | 1 |

the stirring current is 10 A. As can be seen from the figure, the calculated value is basically consistent with the measured value, and the error is very small. The measured value is slightly lower than the calculated value; the reason might be there is a certain magnetic leakage in the actual work of the stirring coil, and part of the equipment is simplified in the model.

Fig. 3 shows the distribution of magnetic field intensity generated by stirring current with and without ingot in the crucible. It can be seen that the distribution of magnetic field in the two cases is basically the same. The stirring magnetic field is mainly distributed in the crucible. The stirring magnetic field in the crucible is large in the middle and small at both ends.

Fig. 4 shows comparison of the distribution of stirring magnetic field intensity on the central axis of the crucible with

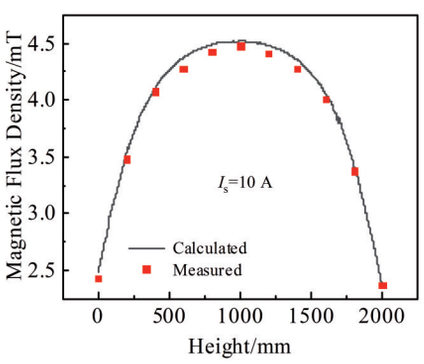


Fig.2 Comparison of the calculated and measured magnetic field intensity on the central axis without ingot in the crucible

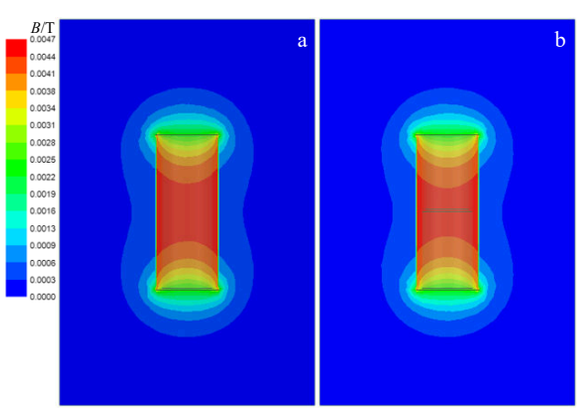


Fig.3 Comparison of magnetic field distribution in crucible without (a) and with (b) ingot

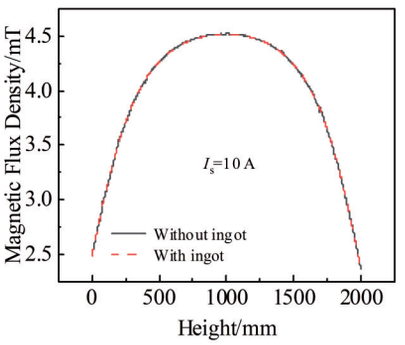


Fig.4 Comparison of magnetic field intensity on the central axis of crucible with and without ingot

and without ingot in the model. It can be seen that the distribution of magnetic field intensity in the two cases is basically the same. The magnetic field intensity at the center of the crucible with ingot is 4.517 mT, which is only 0.005 mT lower than that without ingot in the crucible. This is because although the conductive molten pool has a certain shielding effect on the magnetic field, the conductivity of the molten pool is much lower than that of the crucible copper tube, and the shielding effect of the molten pool on the electromagnetic field can be ignored. This also indicates that the magnetic field strength measured without ingot can represent the data of normal production with ingot. In the following calculations there are ingots in the crucible.

## 3 Results and Discussion

### 3.1 Current distribution changes with or without stirring magnetic field

Fig. 5 shows the current distribution changes in crucible, ingot and electrode without stirring magnetic field. As can be seen from the figure, since the cross-sectional area of the ingot is much larger than that of the crucible, the current density in

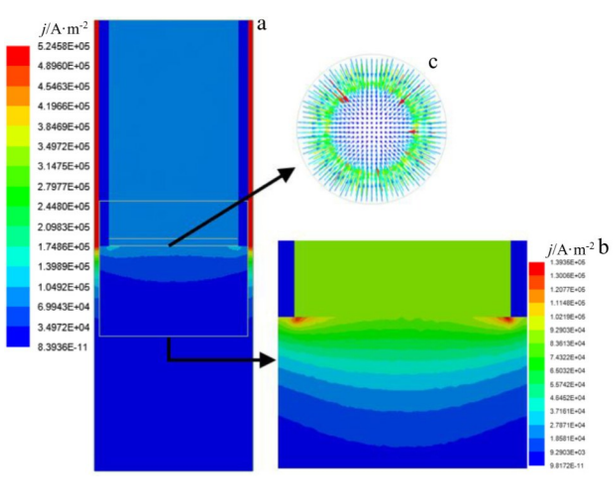


Fig.5 Current distribution in crucible, ingot and electrode without stirring magnetic field: (a) total distribution, (b) contact area between ingot and electrode, and (c) current vector diagram on the upper surface of ingot

the crucible is much larger than that in the ingot and electrode (Fig.5a). The current distribution is uniform when the crucible is not in contact with the ingot, and the current distribution in the electrode is also uniform (Fig.5a). When the crucible is in contact with the ingot, the current flows to the electrode through the ingot in the shortest path, and the maximum current forms at the contact between the ingot and the arc zone (Fig. 5b). The surface current of the ingot is the largest, and the current decreases rapidly downward along the ingot. There is almost no current distribution in a large area of the lower part of the ingot (Fig. 5a and 5b). The current is centripetally distributed from the crucible through the ingot to the crucible (Fig.5c).

Fig. 6 shows the current distribution changes in the ingot and electrode with and without stirring magnetic field. It can be seen that the current distribution in the ingot and electrode with and without stirring magnetic field is almost the same. The current in the ingot is concentrated within 350 mm of the upper part of the ingot. The maximum surface current of ingot under stirring magnetic field increases slightly compared with that without stirring magnetic field. In both cases, the current on the ingot surface is distributed centripetally.

### 3.2 Magnetic field distribution in ingot and electrode with or without stirring magnetic field

Fig. 7 shows the variation of magnetic field distribution in the ingot and electrode with and without stirring magnetic field. Without stirring magnetic field, the self-inductive magnetic field generated by the melting current is mainly distributed inside the crucible, matching the current distribution, and there is almost no magnetic field at the bottom of the ingot. Since the current direction of the crucible and the electrode is opposite, the magnetic field in the middle of the electrode offsets each other, and the magnetic field intensity increases gradually from the center to the edge. When applying a stirring current, the stirring current magnetic field and the melting current magnetic field are coupled. From the magnetic field vector diagram of the upper surface of the ingot, it can be seen that the magnetic fields of them rotate counterclockwise. The magnetic field is mainly distributed along the tangential direction, and the radial component is almost zero. When applying a stirring magnetic field, the magnetic field vector has a axial component.

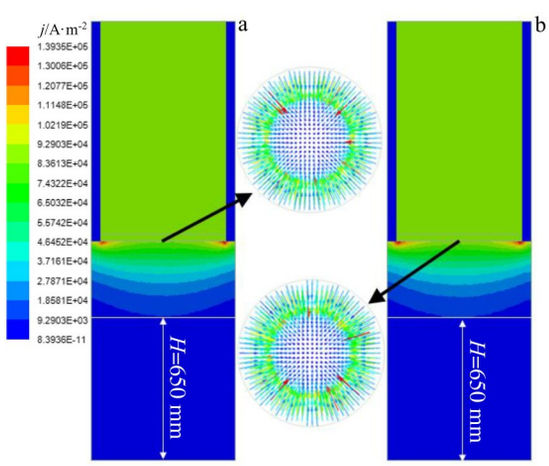


Fig.6 Comparison of current distribution in ingot and electrode with (a) and without (b) stirring magnetic field

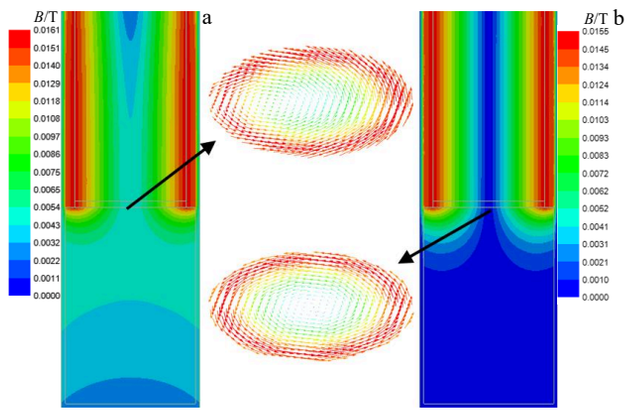


Fig.7 Magnetic field distribution in ingot and electrode with (a) and without (b) stirring magnetic field

Fig. 8 shows the distribution of magnetic field intensity along the *y*-axis diameter direction on the upper surface of the ingot with and without stirring magnetic field. Since the distribution of magnetic field strength in the radial direction is almost zero, only the tangential and axial magnetic field strength are given in the diagram. It can be seen that the tangential component distribution of magnetic field is almost the same whether there is stirring magnetic field. As the radius increases, the magnetic field strength gradually increases, reaching a maximum of 15.1 mT when the radius $R$ is 285 mm, and then gradually decreases. When there is no stirring magnetic field, the axial component of the magnetic field is almost zero. When there is a stirring magnetic field, the axial component of the magnetic field is about 4.5 mT, which is equal to the value at height $H$=1000 mm in Fig.4. Through the above analysis, it can be seen that the stirring current magnetic field and the melting current magnetic field are simply superimposed.

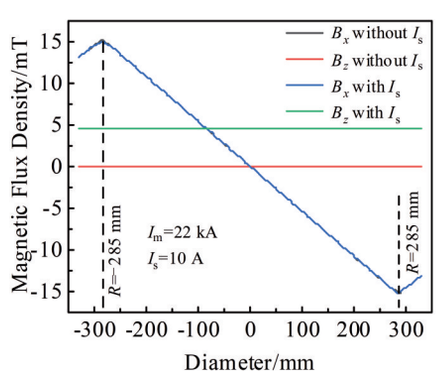


Fig.8 Comparison of magnetic field intensity in the diameter direction of ingot upper surface with and without stirring magnetic field

### 3.3 Variation of electromagnetic force in ingot with and without stirring magnetic field

Fig. 9 shows the electromagnetic force vector distribution on the upper surface of the ingot with and without stirring magnetic field. As can be seen, without stirring magnetic field, the radial electromagnetic force pointing to the center of the ingot is generated under the action of the melting current and its self-induced magnetic field. When there is a stirring magnetic field, the electromagnetic force on the upper surface of the ingot rotates obviously.

In order to analyze the distribution of the electromagnetic force on the upper surface of the ingot, the components of the electromagnetic force along the *y*-axis diameter in *x*, *y* and *z* directions are plotted, as shown in Fig. 10. It can be seen that without stirring magnetic field, the tangential component of the electromagnetic force on the surface of the ingot along the *x*-axis is almost zero. At the radius less than 270 mm, the radial component of the electromagnetic force along the *y*-direction points to the center of the ingot with a linear distribution, and reaches the maximum value at the radius of 270 mm, and then rapidly decreases to 0. The axial component of the electromagnetic force in the *z*-direction points downward and increases with the increase in the radius. It reaches the maximum when the radius is 290 mm, and then gradually decreases. When there is stirring magnetic field, the component of electromagnetic force along *y*- and *z*-direction is the same as the case without stirring magnetic field. At the same time, the tangential electromagnetic force along the *x*-direction is generated under the action of stirring magnetic field, and the electromagnetic force gradually increases with the increase in radius.

Fig. 11 shows the change of total electromagnetic force on ingot diameter with height. It can be seen that the electromagnetic force on the surface of the ingot gradually increases along the radius direction, reaching the maximum value when the radius is 270 mm, and then gradually decreases, which is the same as the variation trend of electromagnetic force in Fig. 10. The electromagnetic force on the upper surface of the ingot is the largest, and decreases rapidly as the height decreases. The electromagnetic force is concentrated in the upper part of the ingot within 200 mm.

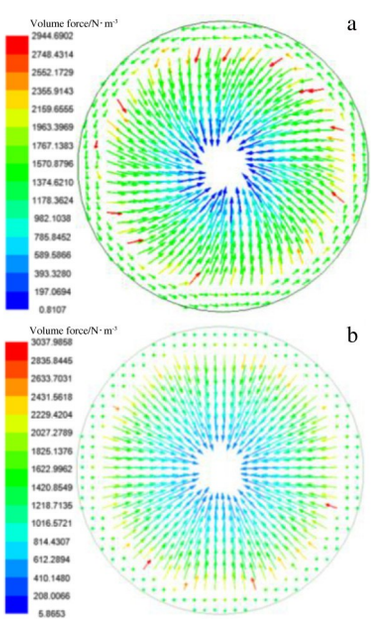


Fig.9 Distribution of electromagnetic force vector on the upper surface of ingot with (a) and without (b) stirring magnetic field

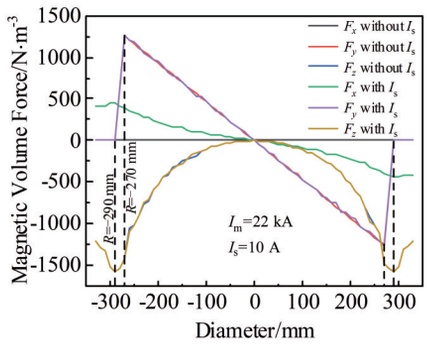


Fig.10 Distribution of electromagnetic force in *y*-axis diameter direction on upper surface with and without stirring magnetic field

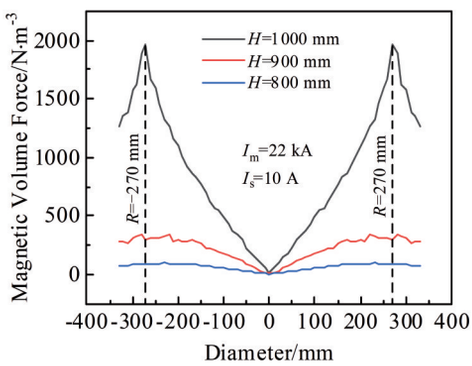


Fig.11 Variation of total electromagnetic force with ingot height

### 3.4 Effect of melting current variation on magnetic field and electromagnetic force

In order to compare the influence of the change of melting current on the magnetic field and electromagnetic force, the current, magnetic field and electromagnetic force distribution were calculated when the melting current was 21, 22 and 23 kA and the stirring current was constant. Fig. 12 shows the current distribution in the ingot and electrode at different melting currents. It can be seen that the current density gradually increases with the increase in the melting current, but the current distribution remains unchanged.

According to the analysis in Section 3.2, the melting current only affects the tangential component of the magnetic field. Fig. 13 shows the change of tangential component of magnetic field on the upper surface of the ingot along the diameter direction. As can be seen, the intensity of the magnetic field increases gradually with the increase in the radius, and

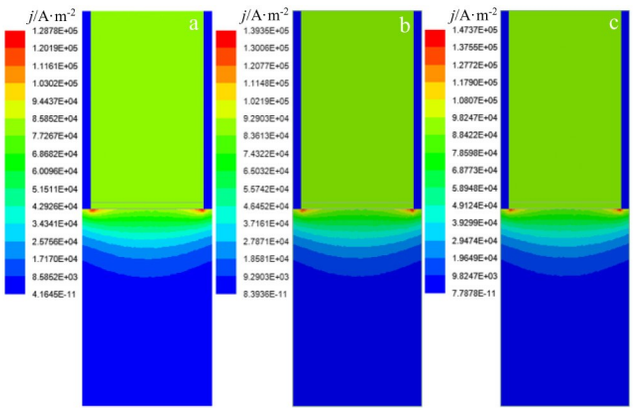


Fig.12 Current distribution in ingot and electrode under different melting currents: (a) $I_m$=21 kA, (b) $I_m$=22 kA, and (c) $I_m$=23 kA

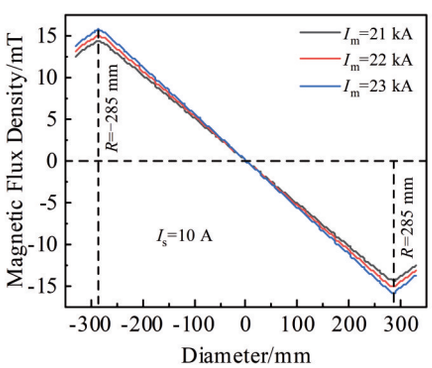


Fig.13 Distribution of tangential component of magnetic field on ingot surface along diameter

reaches the maximum value when the radius $R$=285 mm, and then decreases gradually. When the melting current is 21, 22 and 23 kA, the maximum value of the tangential component of the magnetic field is 14.40, 15.07 and 15.74 mT, respectively, and the increase amount is 0.67 mT, showing a linear change.

According to the analysis in Section 3.3, the melting current has an effect on the radial and axial electromagnetic forces of the ingot, so the sum of the radial and axial electromagnetic forces on the upper surface of the ingot is analyzed, as shown in Fig. 14. The variation trend of electromagnetic force along the diameter direction is basically the same with the increase in melting current, and the maximum value is reached when the radius is 270 mm. When the melting current is 21, 22 and 23 kA, the maximum electromagnetic force is 1740.9, 1925.2 and 2110.2 N/m$^3$, respectively, increased by 184.3 and 185 N/m$^3$, showing a linear change.

### 3.5 Influence of stirring current variation on magnetic field and electromagnetic force

In order to compare the influence of stirring current change on magnetic field and electromagnetic force, the distribution of current, magnetic field and electromagnetic force was calculated when the stirring current was 8, 9 and 10 A

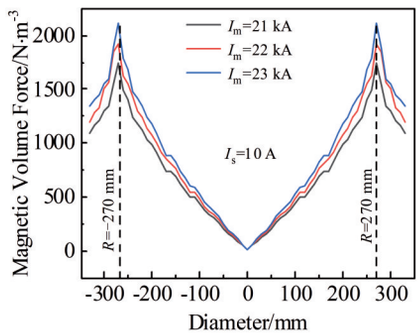


Fig.14 Variation of the sum of radial and axial electromagnetic forces on the upper surface of ingot along the diameter

respectively under the condition of constant melting current. Fig. 15 shows the current distribution in ingot and electrode under different stirring currents. It can be seen that with the increase in stirring current, the current density increases slightly, but the current distribution remains unchanged.

According to the analysis in Section 3.2, stirring current only affects the axial component of the magnetic field. Fig. 16 shows the variation of the axial component of the magnetic field at the center of the ingot surface with the stirring current. As can be seen, when the stirring current is 8, 9 and 10 A, the axial components of the magnetic field are 3.61, 4.06 and 4.51 mT, respectively, and the increment is 0.45 mT, showing a linear change.

According to the analysis of Section 3.3, the stirring current has an effect on the tangential electromagnetic force of the ingot. The tangential electromagnetic force on the upper surface of the ingot is analyzed, as shown in Fig. 17. It can be seen that with the increase in stirring current, the changing trend of the electromagnetic force along the diameter is basically the same, and the maximum value is reached when the radius is 290 mm. When the stirring current is 8, 9 and 10 A, the maximum value of the radial electromagnetic force is 356, 401 and 443 N/m$^3$, respectively, and the increased amount is 45 and 42 N/m$^3$, basically showing a linear change.

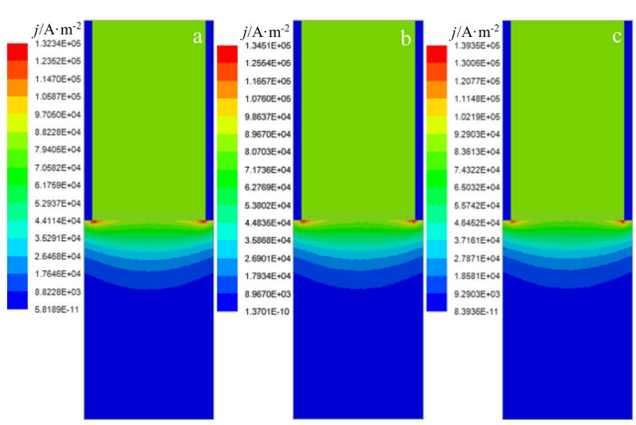


Fig.15 Current distribution in ingot and electrode under different stirring currents

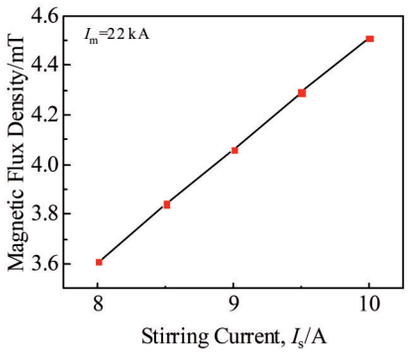


Fig.16 Variation of the axial component of the central magnetic field on upper surface of ingot with stirring current

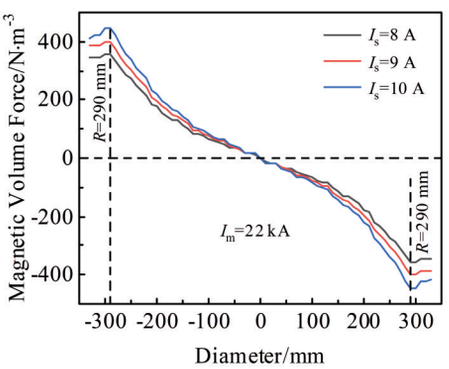


Fig.17 Variation of tangential electromagnetic force on upper surface of ingot along diameter

## 4 Conclusions

1) The current distribution in the ingot and electrode is almost the same with or without stirring magnetic field, and the current distribution in the ingot is concentrated in the upper part of the ingot within 350 mm, and the current distribution in the ingot is centripetal.

2) The melting current produces tangential magnetic field, the stirring current produces axial magnetic field, and the two magnetic fields are simply coupled. The radial magnetic field is almost zero. The intensity of the tangential component of the magnetic field increases gradually with the increase in the radius, reaches the maximum value of 15.1 mT when the radius is 285 mm, and then decreases gradually.

3) Under the action of melting current and its self-induced magnetic field, radial and axial electromagnetic forces are generated. The electromagnetic force rotates under the action of stirring magnetic field, producing tangential electromagnetic force. The radial component of the electromagnetic force points to the center of the ingot and is linearly distributed, which reaches the maximum value when the radius is 270 mm, and then rapidly decreases to 0. The electromagnetic force points downward along the axial component and increases with the increase in the radius, reaching the maximum value when the radius is 290 mm, and then gradually decreases. The tangential component of the electromagnetic force increases gradually with the increase in radius. The electromagnetic force is concentrated in the upper part of the ingot within 200 mm.

## References

1 Guo Li, He Weixia, Zhou Peng *et al. Hot Working Technology*[J], 2020, 49(22): 22

2 Lei Wenguang, Zhao Yongqing, Han Dong *et al. Materials Reports*[J], 2016, 30(3): 101

3 Yuan Wei. *Nonferrous Metals Processing*[J], 2018, 47(2): 23

4 Zou Wuzhuang. *Titanium Industry Progress*[J], 2011, 28(5): 41 (in Chinese)

5 Sun Laixi, Xue Xiangyi, Yang Zhijun *et al. Foundry Technology*[J], 2011, 32(5): 704

6 Chen Qinghong, Xu Shizhen, Jiang Xiaodong. *Materials Protection*[J], 2013, 46(S1): 30 (in Chinese)

7 He Yongsheng, Hu Rui, Luo Wenzhong *et al. Rare Metal Materials and Engineering*[J], 2017, 46(10): 3063 (in Chinese)

8 Qu Jinglong, Yang Shufeng, Chen Zhengyang *et al. China Metallurgy*[J], 2020, 30(1): 1

9 Chang Yan. *Industrial Heating*[J], 2019, 48(5): 21

10 Zhao Xiaohua, Li Jinshan, Chang Hui *et al. The Chinese Journal of Nonferrous Metals*[J], 2010, 20(S1): 539

11 Wang Binbin, Chang Hui, Li Jinshan *et al. Rare Metal Materials and Engineering*[J], 2009, 38(11): 1970 (in Chinese)

12 Li Shaoxiang, Xiao Hong, Wang Pu *et al. Metals*[J], 2019, 9(9): 946

13 Pericleous Koulis, Djambazov Georgi, Ward Mark *et al. Metallurgical and Materials Transactions A*[J], 2013, 44(12): 5365

14 Chapelle P, Jardy A, Bellot P *et al. J Mater Sci*[J], 2008, 43(17): 5734

# 钛合金真空自耗熔炼过程中电流、磁场和电磁力数值模拟

靖振权[1]，孙彦辉[1]，陈　炼[2]，耿乃涛[3]，郑友平[3]，彭　力[3]，王　莹[3]

(1. 北京科技大学 钢铁共性技术协同创新中心，北京 100083)

(2. 攀钢集团攀枝花钢铁研究院有限公司，四川 攀枝花 617000)

(3. 成都先进金属材料产业技术研究院股份有限公司，四川 成都 610300)

**摘　要：**采用有限元模拟软件Ansys Electromagnetics Suite中Maxwell 3D模块建立钛合金真空自耗熔炼过程电磁场数学物理模型，分析并掌握熔炼过程中电流、磁场和电磁力相互作用规律，并研究了熔炼电流和搅拌电流变化对磁场及电磁力的影响。结果表明：铸锭中电流均呈向心分布，且集中分布在铸锭上部350 mm范围内；熔炼电流产生切向磁场，搅拌电流产生轴向磁场，两者进行简单耦合；在熔炼电流及其自感磁场的作用下，产生径向和轴向电磁力；该电磁力又在搅拌磁场的作用下发生旋转，产生切向电磁力；随熔炼电流线性变化，磁场切向分量和电磁力的径向和轴向合力均呈线性变化；随搅拌电流线性变化，磁场轴向分量和电磁力径向分量均呈线性变化。

**关键词：**钛合金；真空自耗熔炼；数值模拟；磁场；电磁力

---

作者简介：靖振权，男，1985年生，博士，北京科技大学钢铁共性技术协同创新中心，北京 100083，E-mail：jingzhenquan@126.com